IEEE Photonics Journal
An IEEE Photonics Society Publication

Open Access

Microwave Photonic Filter by Using Recirculating Frequency Shifter to Generate Optical Frequency Comb

Volume 13, Number 2, April 2021

Weiyu Dai
Weiying Rao
Haoran Wang
Hongyan Fu, *Member, IEEE*

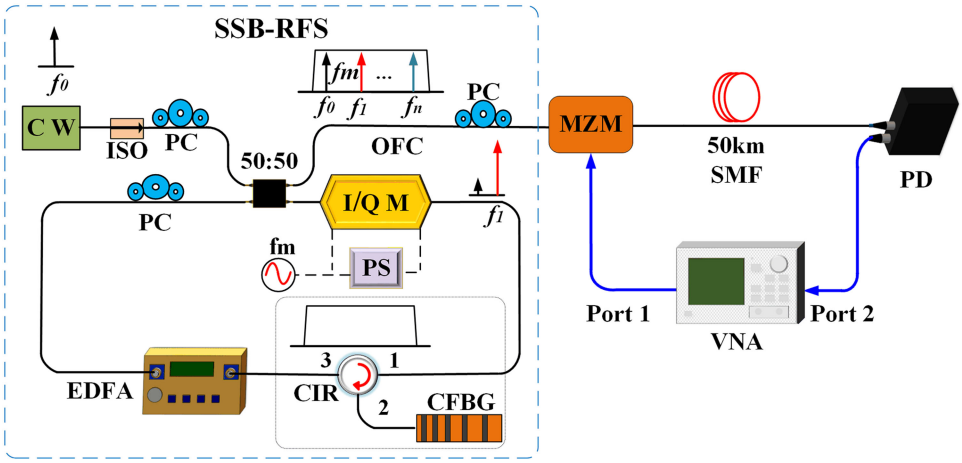

DOI: 10.1109/JPHOT.2021.3069104

Microwave Photonic Filter by Using Recirculating Frequency Shifter to Generate Optical Frequency Comb

Weiyu Dai, Weiying Rao, Haoran Wang, and Hongyan Fu, *Member, IEEE*

Department of Electronic Engineering, School of Electronic Science and Engineering (National Model Microelectronics College), Xiamen University, Xiamen 361005, China

DOI:10.1109/JPHOT.2021.3069104

Manuscript received January 4, 2021; revised March 23, 2021; accepted March 24, 2021. Date of publication March 26, 2021; date of current version April 13, 2021. This work was supported by the National Natural Science Foundation of China under Grant 61975167. Corresponding author: Hongyan Fu (e-mail: fuhongyan@xmu.edu.cn).

Abstract: In this paper, a continuously tunable microwave photonic filter (MPF) with optical frequency comb (OFC) generated by recirculating frequency shifter (RFS) based on an inphase/quadrature (I/Q) modulator is proposed and experimentally demonstrated. A chirped fiber Bragg grating (CFBG) is inserted into the RFS loop to act as an optical bandpass filter. The central frequencies of two passbands of the MPF in 20 GHz range have been tuned linearly from 7.67 GHz to 9.04 GHz, and 15.34 GHz to 18.03 GHz, respectively by changing the frequency of the driving microwave signal onto the I/Q modulator from 20 GHz to 17 GHz. When the frequency of the driving microwave signal is decreased, OFC with smaller tone spacing is generated, and then the MPF's passbands move to higher frequency. So that, the proposed MPF's passbands with high frequencies can be achieved by applying driving microwave signal with low frequency to generate the OFC. By varying the bandwidth of the CFBG, the number of comb lines can be changed, which results in different bandwidth of the MPF's passband. Furthermore, in our experiment by carefully adjusting bias voltage of the Mach-Zenhder modulator, when the frequencies of driving microwave signal onto the I/Q modulator is 20 GHz and 18 GHz, one passband in the 20 GHz range can be suppressed at the frequency of 15.34 GHz, and 8.52 GHz, respectively.

Index Terms: I/Q modulator, microwave photonics filters, optical frequency comb, chirped fiber Bragg grating.

1. Introduction

Microwave photonic filters (MPF) have attracted much research attention due to their advantages such as large bandwidth, low loss, immunity to electromagnetic interference, good tunability and reconfigurability and so on, which are difficult to be achieved with traditional electronic technology [1]–[5]. Fifth generation (5G) cellular systems are required to provide gigabit wireless data rate, supporting bandwidth-intensive applications such as streaming and cloud computing, on mobile devices [6]. For high radio frequency, it is difficult to tune the RF filter with large bandwidth, while it is easier to realize large-scale tuning when it is converted to the optical field [7]. MPFs with freely adjustable passbands and high Q value are desired for 5G transmission, which need low delay, wide coverage, and large network capacity [8].

MPF based on multiple optical source and dispersive medium is one important way for MPF implementation. In literature, laser light source array [9], Fabry-Perot laser [10], optical frequency

comb [11]–[14] and sliced broadband source [15] have been used to construct multi-source MPFs [16]. Optical frequency combs provide a much stable frequency carriers and is a kind of high quality optical source, compared with other multi-wavelength sources for MPF implementation. An MPF based on cascaded modulators to generate optical frequency comb has been reported [11], in which high-power RF amplifier are needed, which increases the complexity and the system cost. The flatness of comb produced by micro-resonator [17] is not good enough for MPF implementation. The optical frequency comb generated by recirculating frequency shifter based on single-sideband modulation (SSB-RFS) loop has many advantages e.g., this structure can provide an adjustable carrier frequency spacing determined by the frequency of the driving RF signal. In addition, the scheme has a good flatness and low driving RF signal power, and it is simple to realize high quality multi-wavelength optical carrier. Large-tap MPF based on optical frequency comb is firstly proposed in [18], and the scheme based on RFS loop is proposed and the central frequency of the MPF can be tuned in 10 GHz [19]. By programming the shape of generated OFC, the combs with flat-top, Gaussian, and Sinc shapes result in MPF's passbands with Sinc, Gaussian, and flat-top shapes, respectively [20]. By compensating the fourth-order dispersion in delay line elements, an MPF with sub-GHz bandwidth based on all fiber parametric comb has been realized [21]. The performance improvement of OFC based MPF by using machine learning technology has been proposed and demonstrated, which makes the OFC-based MPF more suitable for practical applications [22].

In this paper, an MPF by using an SSB-RFS based OFC and a dispersive medium has been proposed and experimentally demonstrated. A chirped fiber Bragg grating (CFBG) is inserted into the SSB-RFS to act as an optical bandpass filter. The generated OFC is used as the multi-wavelength light source to implement MPF together with a dispersive medium. Three CFBGs with different bandwidth have been adopted to implement MPFs with different bandwidth. Both theoretical and experimental studies have been carried out, which show good agreement. The central frequencies of MPF's passbands can be tuned by changing the frequency of the driving microwave signal of the OFC, which shows good tuning linearity. Furthermore, by decreasing the frequency of the driving microwave signal onto the I/Q modulator, the frequencies of the MPF's passbands move to higher frequency, which means that MPF with high frequency passbands can be achieved by just adopting low frequency driving signal in the OFC. What's more, together with the carrier suppression effect (CSE) of the MZM, one of the passbands in 20 GHz range can be suppressed by carefully adjusting the bias voltage of the Mach-Zehnder modulator (MZM), and in our experiment with the frequency of 18 GHz and 20 GHz for the driving microwave signal of the OFC, passbands at 15.34 GHz and 8.52 GHz can be suppressed, respectively. The proposed MPF exhibits narrow bandwidth, can be easily tuned with good tuning linearity, and switchable passbands to certain extent, and thus shows potentials for system applications.

2. Theoretical Principle

Fig. 1 illustrates the schematic diagram of the proposed MPF based on OFC generated by SSB-RFS, whose schematic diagram is shown in the blue dashed box. The SSB-RFS includes a CW laser, a 3 dB coupler, an I/Q modulator, an erbium doped fiber amplifier (EDFA), a CFBG and a polarization controller (PC). Microwave signal with the frequency f_m is splitted to two branches, and applied onto I and Q channels of the I/Q modulator, respectively, and a phase shifter (PS) is inserted in one of the channels. To satisfy the single sideband modulation (SSB) conditions, two arms are biased at their null points ($V_{BI} = V_{BQ} = V_\pi$) and modulated by orthogonal RF signals, where V_{BI} and V_{BQ} are the bias voltage of the I and Q channel. The channels I and Q have the phase differences $\varphi = -\frac{\pi}{2}$ introduced by the phase modulator in the I/Q modulator. Then the transfer function of the I/Q modulator based on SSB can be expressed as follows [14]:

$$T = \frac{1}{2}\left[\sin\left(\frac{\pi}{2}\cdot\frac{V_I(\mathrm{t})}{V_\pi}\right) + j\cdot\sin\left(\frac{\pi}{2}\cdot\frac{V_Q(\mathrm{t})}{V_\pi}\right)\right] \tag{1}$$

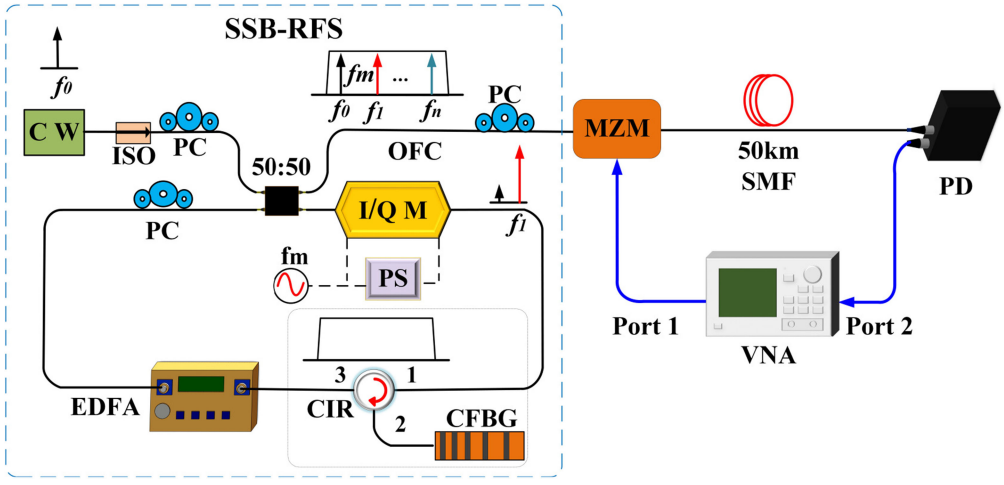

Fig. 1. The schematic diagram of the proposed MPF based on OFC and a dispersive medium; the blue dashed box: the OFC generation based on SSB-RFS; PC: polarization controller; I/Q M: I Q modulator; PS: phase shifter; EDFA: Erbium doped fiber amplifier; CFBG: Chirped Fiber Bragg grating; CIR: circulator; MZM: Mach-Zehnder modulator; VNA: vector network analyzer; PD: photodetector.

where $V_I(t) = V_m \cos(2\pi f_m t)$and $V_Q(t) = V_m \sin(2\pi f_m t)$ are the microwave signals applied on the arms of channels I and Q of the I/Q modulator, whose phase difference is $\frac{\pi}{2}$ introduced by the PS. V_m and V_π are the voltage peak value of microwave signal and the half-wave voltage of the modulator. The seed CW light with central frequency f_0 can be represented as $E_I = E_0 \exp(j2\pi f_0 t)$, and the output light field after the first round trip of the I/Q modulator can be expressed as [23]:

$$E_{\text{out}} = \frac{1}{2} E_0 \exp(j2\pi f_0 t) \cdot \left\{ \sin\left[\frac{\pi}{2} \frac{V_m \cos(2\pi f_m t)}{V_\pi} \right] + j \cdot \sin\left[\frac{\pi}{2} \frac{V_m \cos(2\pi f_m t)}{V_\pi} \right] \right\} \tag{2}$$

By using the Jacobi–Anger expansion, the above equation can be expressed as:

$$\begin{aligned} E_{\text{out}} = E_0 \exp(j2\pi f_0 t) \cdot \Bigg\{ & j^{2k-2} \cdot \sum_{k=1}^{\infty} J_{2k-1}\left(\frac{\pi V_m}{2V_\pi} \right) \cos[(2k-1)2\pi f_m t] \\ & + j \sum_{k=1}^{\infty} J_{2k-1}\left(\frac{\pi V_m}{2V_\pi} \right) \sin[(2k-1)2\pi f_m t] \Bigg\} \\ = E_0 \exp(j2\pi f_0 t) \cdot & [J_1(m) \cdot \exp(j2\pi f_m t) - J_3(m) \cdot \exp(-j6\pi f_m t) + J_5(m) \cdot \exp(j10\pi f_m t) - \ldots] \end{aligned} \tag{3}$$

where $m = \frac{\pi V_m}{2V_\pi}$ denotes the modulation depth. The crosstalk comes from the third-order harmonics and above harmonics. The output electronic field of I/Q modulator can be expressed as $E_{out} \propto E_0 \exp[j2\pi(f_0 + f_m)t]$, when the first-order harmonic are large enough and the harmonics over the third-order are small enough and can be neglected. The shifted optical signal ($f_n = f_0 + \text{nf}_\text{m}$) ($n$ represents the number of comb lines of the SSB-RFS based OFC) is amplified by the EDFA to compensate the modulation loss and insertion loss with inevitable ASE noise accumulation, which can be suppressed by the CFBG in the RFS loop. The CFBG can also be used to control the desired carrier number with the bandwidth of $B = \text{n} \cdot f_m$, which can also be given by:

$$B = C_g \cdot z \tag{4}$$

where C_g is the chirp coefficient, and z is the length of the total fiber grating. By carefully adjusting the PC and the bias voltage applied to the I/Q modulator, we can obtain OFC with nearly flat spectrum by n round trip.

The OFC generated by SSB-RFS serves as the optical source of the MPF, which is modulated by microwave signal from port 1 of vector network analyzer (VNA) after a PC via an MZM. The modulated light is launched into the dispersive medium which is a coil of 50 km single-mode fiber (SMF) in our experiment to perform sampling and time delay. Then the light is transmitted to the photodiode (PD) and the recovered signal is sent to port 2 of the VNA for measurement. The amplitude response of the MPF $|H(f_{RF})|$ can be obtained by applying Furrier transform to its photocurrent, which is the multiplication of $E_{out}(t)$ and its conjugate as follows [22], [24]:

$$\left|H(f_{RF})\right| \propto \left|\sum_{n=1}^{N} P_n \exp[-j2\pi \cdot f_{RF}(n-1)D(\lambda)\cdot\Delta\lambda]\right| \cdot \cos\left(\frac{\pi\lambda_0{}^2 D(\lambda)}{c}\frac{f_{RF}^2}{2}\right) \tag{5}$$

where $D(\lambda)$ is the dispersion (unit: ps/nm) of the dispersive fiber, P_n is the output power of the n-th tone of the OFC, λ_0 is the central wavelength and $\Delta\lambda$ is the wavelength spacing between the adjacent comb lines. c is the velocity of light in the vacuum and f_{RF} is the frequency of the microwave signal added to MZM. The OFC based MPF exhibits periodic frequency response, and the free spectrum range (FSR) of the OFC based MPF can be given by [24]:

$$FSR = \frac{1}{D(\lambda)\cdot\Delta\lambda} \tag{6}$$

The number of comb lines n is controlled by the bandwidth of CFBG, while the wavelength spacing ($\Delta\lambda$) depends on the frequency (f_m) of the microwave signal applied on the I/Q modulator. These are two important factors for tunability and configurability of the proposed OFC based MPF.

3. Experimental Results and Discussions

In the experiment, the center wavelength of the CW laser is 1549.403 nm. The frequency shift of the RFS loop depends on the frequency of the microwave signal applied onto the I/Q modulator, which in the first experiment is set at 20 GHz. In our experiment, three CFBGs with different bandwidth, 5 nm, 8 nm and 10 nm have been used as the optical bandpass filter in the RFS loop, respectively. The simulated and measured optical spectra of the SSB-RFS based OFC by using CFBGs with different bandwidth are shown as Fig. 2(a) and (b), and the corresponding calculated and measured frequency response of the proposed MPF is shown in Fig. 2(c) and (d), respectively.

These CFBGs have steep edges and deep depth, which make it applicable to implement OFC with good flatness and high rejection ratio. One can see from Fig. 2(a) and (b) that, OFC with 31-lines 50-lines and 63-lines can be obtained by using CFBGs with bandwidth of 5 nm, 8 nm and 10 nm, respectively. The number of comb lines depends on the bandwidth of the CFBG in the RFS loop when the frequency of the driving microwave signal is fixed. The carrier-to-noise ratio (CNR) are estimated to be ∼15.53 dB, ∼19.76 dB, and ∼20.63 dB, respectively, and the flatness of the OFC are less than 3 dB in both simulation and experimental results. The simulated and measured frequency response of the MPF are shown in Fig. 2(c) and (d). For the simulation results, since the noise factor caused by amplified spontaneous radiation is not considered, the spectrum has a higher CNR and better frequency response compared with the experimental results. The central frequency, the extinction ratio and the 3dB bandwidth of the first passband are 7.67 GHz, 17.8 dB and 162.49 MHz, respectively, and the central frequency of the second passband are 15.34 GHz when the bandwidth of the CFBG is 10 nm. When the bandwidth of the CFBG is set at 5 nm, the 3dB bandwidth of the first passband of the OFC based MPF is ∼224.99 MHz. This is because that CFBG with larger optical bandwidth can provide a larger number of comb lines and then larger number of taps for the MPF, so that MPF with narrower passbands can be obtained.

When the frequency of the driving microwave signal is changed, the wavelength spacing of the comb lines will be tuned, and thus the OFC based MPF is tunable. In our experiment, when the frequency of driving microwave signal is set at 20 GHz to 17 GHz, the measured frequency response of the MPF is depicted in Fig. 3(a)–(d), from which one can see that two passbands of the MPF has been tuned linearly from 7.67 GHz to 9.04 GHz, and 15.34 GHz to 18.03 GHz, respectively. The

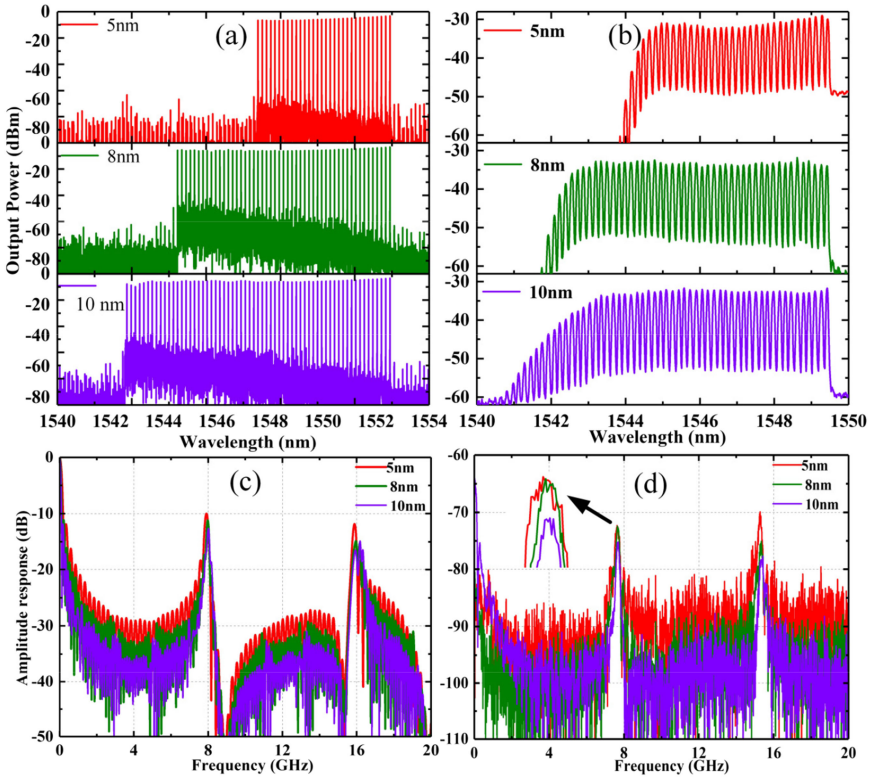

Fig. 2. The simulated (a) and the measured (b) spectra of the SSB-RFS based OFC when the bandwidth of CFBGs are 5 nm, 8 nm and 10nm respectively; the simulated (c) and the measured (d) frequency response of the MPF with the corresponding OFC as the optical source.

extinction ratio of the MPF's passbands is more than 13 dB. The relationship between the central frequencies of the MPF's passbands and the frequency of the driving microwave signal is shown in Fig. 3(f), which shows good tuning linearity. Since double sideband modulation is employed in our experiment, dispersion induced microwave power fading will have influences on the tunability feature of the MPF, and by adjusting the bias voltage onto the MZM, the suppression points of the dispersion induced power fading can be changed, which enable a continuous tunability of the proposed OFC based MPF. One can see from the results that with the decrease of the driving frequency, the central frequencies of both passbands are increased. Fig. 3(e) shows that, when the frequency of the driving signal is 15 GHz, the frequency of the MPF's second passbands is higher than 20 GHz, so that we cannot measure it due to the measurement range of the VNA. In our experiment, microwave signal with the frequency higher than 15 GHz has been adopted to the MPF implementation for the sake of measurement; however, in applications, MPF with higher frequency passbands can be achieved by applying driving microwave signal with lower frequency, which is beneficial for the system application.

In our experiment, for some modulation frequencies of the driving microwave signal onto the I/Q modulator, by carefully adjusting the bias voltage of the MZM, one of the passbands can be suppressed in the 20 GHz range. When the frequency of the driving microwave signal is 18 GHz, one can see from Fig. 4(a) and (c) that, the first passband can be suppressed with the bias voltage set at 1.4 V, while the frequency response exhibits two passbands in 20 GHz range with the bias voltage set at 2.6 V. When the driving frequency is 20 GHz, the second passband can be suppressed with the bias voltage set at 3.6 V, while there are two passbands when the bias voltage is set at 2.4 V, which results are shown as Fig. 4(b) and (d). This switchable characteristic is mainly caused by the carrier suppression effect (CSE) of the double sideband modulation (DSB)

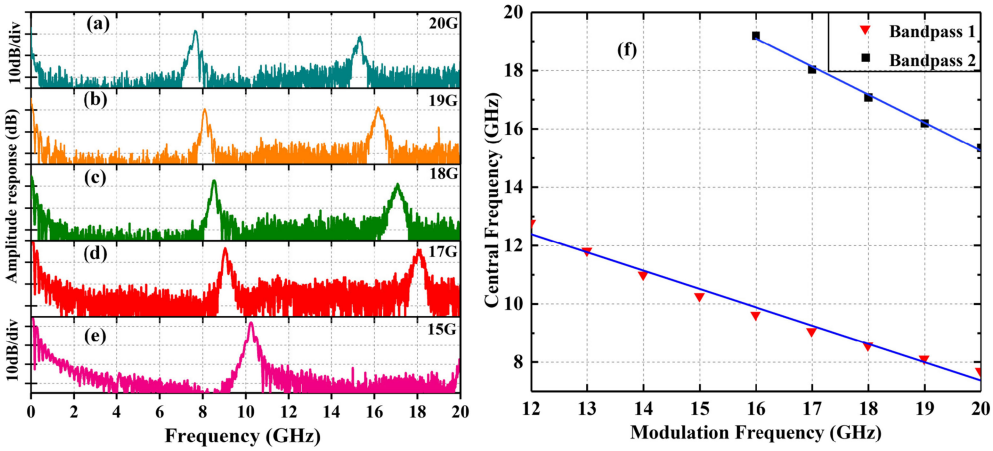

Fig. 3. The measured frequency response (a)–(e) of the OFC based MPF when the frequencies of the driving microwave signal are set at 20 GHz to 17 GHz, and 15 GHz, respectively; the relationship between the central frequencies of MPF's passbands and modulation frequency (f).

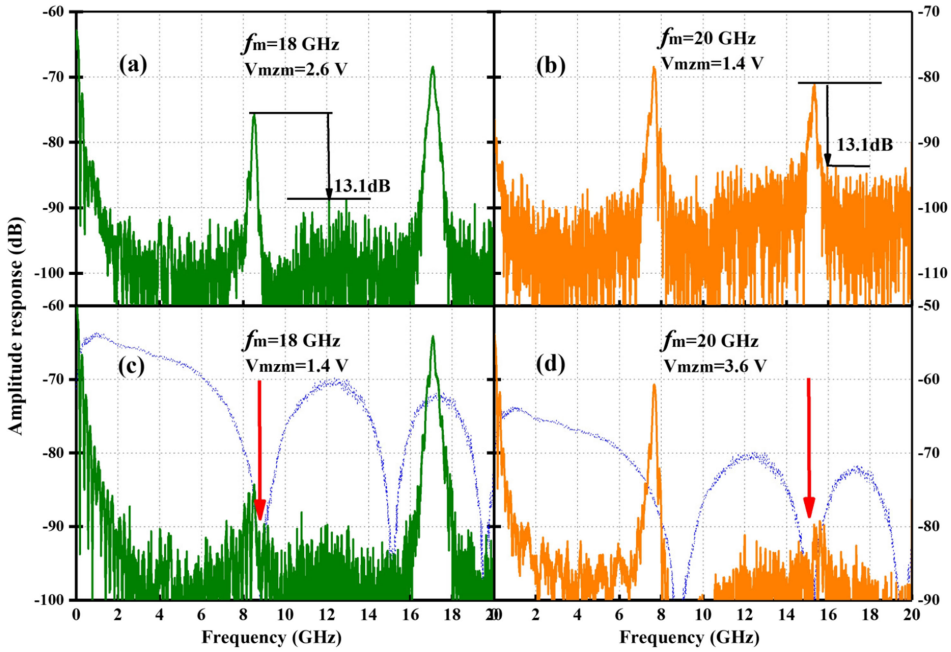

Fig. 4. The measured frequency response when the driving frequency is 18 GHz (a) (c) and 20 GHz (b) (d), with different bias voltage applied on the MZM. The dashed line is the CSE curve.

of the MZM, which curve is plotted as the dashed blue lines in Fig. 4(c) and (d) with no driving signal is applied on the I/Q modulator. When the frequencies of MPF's passbands coincide with the CSE induced notch frequencies, the passbands can be suppressed. In our experiment, the first and second notch frequencies of the CSE curve are located at 8.78 GHz and 15.13 GHz, respectively, which coincide with the first and second passband when the frequencies of the driving microwave signal on the I/Q modulator are 18 GHz, and 20 GHz, respectively. So that, one of the passbands has been suppressed, as one can see in Fig. 4(c) and (d). When the bias of the MZM is changed, the notch depth will also vary accordingly [25], and thus the amplitude of the suppressed passbands. Especially, when the odd/even order of modulation sidebands are suppressed by

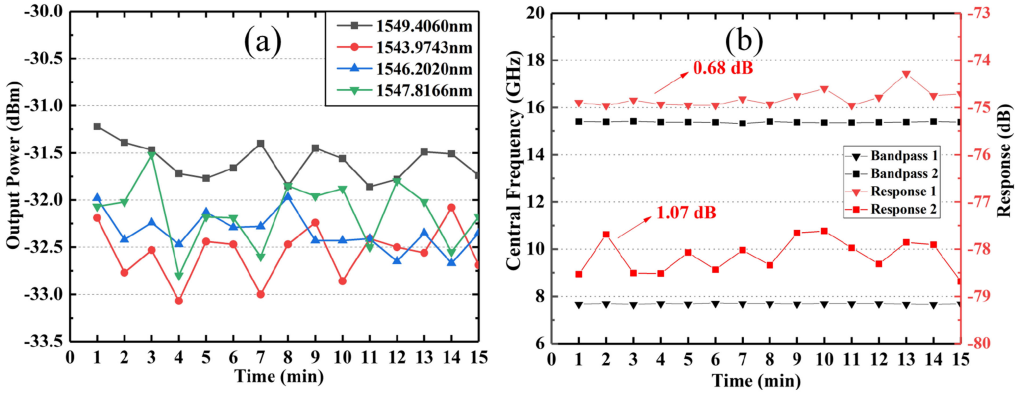

Fig. 5. (a) The power fluctuation of four comb lines of the SSB-RFS OFC within 15 minutes; (b) The stability of central frequency and the power of the OFC based MPF's passbands within 15 minutes.

changing the bias voltage, the notch frequencies of the CSE curve will be different from that of DSB condition. As a result, those passbands above will not coincide with the notch frequencies anymore and two passbands can be observed in 20 GHz range, shown as Fig. 4(a) and (b). This switching characteristics can be applied in some occasions that the system operation state needs to be switched between two-channel state and one-channel state, e.g., in some satellite communication system, MPF is required to have passband switchable function to enable two passbands or only one passband, depending on the application scenario [26].

In addition, in our experiment we have measured the power stability of four selected comb lines every 1 min within a 15 minutes range, which is shown Fig. 5(a). One can see that the power fluctuation of the 4 comb lines is less than 1.28 dB, so the OFC has good power stability. We have also measured the stability of the central frequencies and power of the MPF's passbands in 15 minutes with the interval of 1 min, which is displayed in Fig. 5(b). It can be seen from the experimental results that, the power fluctuations of the MPF based OFC are 0.68 dB and 1.07 dB, respectively, while the central frequency instability of the two passbands are ∼50 MHz and ∼100 MHz, respectively. The main reasons of the fluctuation are the jitter of the light source, the power instability of the RF source, the bias voltage drift of the modulator and the accumulation of EDFA spontaneous emission noise. The OFC's spectrum and the ASE noise accumulated in RFS loop will limit the MPF's performance. A programmable optical filter can be employed in the RFS loop to reduce the ASE noise. In our experiment, a bundle of 50 km SMF has been used as a dispersion medium, which introduces large insertion loss for the MPF. To reduce the loss, A CFBG with designed dispersion characteristics which has small insertion loss can be used instead of the SMF. What's more, windowing techniques can also be used to tailor the MPF's coefficients for increasing the suppression ratio and configurability of the MPF [27].

4. Conclusion

In conclusion, an MPF by using an SSB-RFS based OFC has been experimentally presented. A CFBG is used to act as an optical bandpass filter in the SSB-RFS loop based on I/Q modulator to generate the OFC, which is used as the multiple optical source to implement the MPF together with a dispersive medium. Three CFBGs with different bandwidth have been used to implement MPFs, respectively, and by using CFBG with larger bandwidth, MPF with narrower bandwidth can be obtained. The central frequencies of MPF's passbands can be tuned by changing the frequency of the driving microwave signal applied onto the I/Q modulator. By decreasing the frequency of the driving microwave signal, the frequencies of the MPF's passbands move to higher frequency, which means that MPF with high frequency passbands can be achieved just by adopting low frequency driving signal for the OFC generation. What's more, in our experiment, together with the CSE of

the MZM, with the frequency of 18 GHz and 20 GHz for the driving microwave signal applied on the I/Q modulator, passbands at 8.52 GHz and 15.34 GHz can be suppressed, respectively by carefully adjusting the bias voltage of the MZM. The proposed MPF shows good performance such as narrow bandwidth, good tuning linearity and selectable passbands for certain frequencies, and thus shows potentials for system applications.

References

[1] A. Akhlaq, A. I. Sulyman, H. Hassanein, A. Alsanie, and S. A. Alshebeili, "Performance analysis of relay-multiplexing scheme in cellular systems employing massive multiple-input multiple-output antennas," *Iet Commun.*, vol. 8, no. 10, pp. 1788–1799, 2014.

[2] W. R. Peltier, "Global glacial isostasy and the surface of the ice-age earth: The ICE-5G (VM2) model and GRACE," *Annu. Rev. Earth Planet. Sci.*, vol. 20, no. 32, pp. 111–149, 2004.

[3] W. Roh *et al.*, "Millimeter-wave beamforming as an enabling technology for 5G cellular communications: Theoretical feasibility and prototype results," *IEEE Commun. Mag.*, vol. 52, no. 2, pp. 106–113, Feb. 2014.

[4] J. Ca Pmany, B. Ortega, and D. Pastor, "A tutorial on microwave photonic filters," *Lightw. Technol. J.*, vol. 24, no. 1, pp. 201–229, 2006.

[5] F. Zeng and J. Yao, "All-optical bandpass microwave filter based on an electro-optic phase modulator," *Opt. Exp.*, vol. 12, no. 16, pp. 3814–3819, 2004.

[6] M. N. Tehrani, M. Uysal, and H. Yanikomeroglu, "Device-to-device communication in 5G cellular networks: Challenges, solutions, and future directions," *IEEE Commun. Mag.*, vol. 52, no. 5, pp. 86–92, May 2014.

[7] A. Kanno *et al.*, "Coherent terahertz wireless signal transmission using advanced optical fiber communication technology," *J. Infrared, Millimeter Terahertz Waves*, vol. 36, no. 2, pp. 180–197, 2015.

[8] T. Udem, R. Holzwarth, and T. Hänsch, "Femtosecond optical frequency combs," *Eur. Phys. J. Special Top.*, vol. 172, no. 1, pp. 69–79, 2009.

[9] A. Loayssa, J. Capmany, M. Sagues, and J. Mora, "Demonstration of incoherent microwave photonic filters with all-optical complex coefficients," *IEEE Photon. Technol. Lett.*, vol. 18, no. 16, pp. 1744–1746, Aug. 2006.

[10] F. Jiang, Y. Yu, H. Tang, L. Xu, and X. Zhang, "Tunable bandpass microwave photonic filter with ultrahigh stopband attenuation and skirt selectivity," *Opt. Exp.*, vol. 24, no. 16, pp. 18655–18663, 2016.

[11] V. R. Supradeepa, C. M. Long, W. Rui, F. Ferdous, and A. M. Weiner, "Comb-based radiofrequency photonic filters with rapid tunability and high selectivity," *Nat. Photon.*, vol. 6, no. 3, pp. 186–194, 2012.

[12] J. Zhang *et al.*, "Improved multicarriers generation by using multifrequency shifting recirculating loop," *Photon. Technol. Lett. IEEE*, vol. 24, no. 16, pp. 1405–1408, Aug. 2012.

[13] J. Zhang, J. Yu, N. Chi, Z. Dong, and L. Tao, "Multichannel optical frequency-locked multicarrier source generation based on multichannel recirculation frequency shifter loop," *Opt. Lett.*, vol. 37, no. 22, pp. 4714–4716, 2012.

[14] Feng *et al.*, "Generation of 50 stable frequency-locked optical carriers for tb/s multicarrier optical transmission using a recirculating frequency shifter," *Lightw. Technol., J.*, vol. 29, no. 8, pp. 1085–1091, 2011.

[15] H. Fu, Z. Xu, and K. Zhu, "Remote wideband microwave frequency measurement based on a single-passband microwave photonic filter," *IEEE Photon. J.*, vol. 4, no. 5, pp. 1401–1406, Oct. 2012.

[16] E. Hamid, W. Rui, V. R. Supradeepa, C. M. Long, and A. M. Weiner, "Tunable radio frequency photonic filter based on intensity modulation of optical combs," in *Proc. Topical Meeting Microw. Photon.*, 2010, pp. 393–396.

[17] P. Del'Haye, A. Schliesser, O. Arcizet, T. Wilken, R. Holzwarth, and T. J. Kippenberg, "Optical frequency comb generation from a monolithic microresonator," *Nature*, vol. 450, no. 7173, pp. 1214–1217, 2007.

[18] E. Hamidi, D. E. Leaird, and A. M. Weiner, "Tunable programmable microwave photonic filters based on an optical frequency comb," *IEEE Trans. Microw. Theory Techn.*, vol. 58, no. 11, pp. 3269–3278, Nov. 2010.

[19] J. Wang, M. Chen, H. Chen, S. Yang, and S. Xie, "Large-tap microwave photonics filter based on recirculating frequency shifting loop," *Photon. Technol. Lett. IEEE*, vol. 26, no. 12, pp. 1219–1222, Jun. 2014.

[20] H. J. Kim, D. E. Leaird, and A. M. Weiner, "Rapidly tunable dual-comb rf photonic filter for ultrabroadband rf spread spectrum applications," *IEEE Trans. Microw. Theory Techn.*, vol. 64, no. 10, pp. 3351–3362, Oct. 2016.

[21] Z. Serahati, E. Temprana, E. Myslivets, V. Ataie, and S. Radic, "Demonstration of a sub-ghz flat-top rf-photonic filter enabled by fourth-order dispersion compensation," *J. Lightw. Technol.*, vol. 38, no. 6, pp. 1194–1201, 2020.

[22] R. K. Shiu, Y. W. Chen, P. C. Peng, J. Chiu, and G. K. Chang, "Performance enhancement of optical comb based microwave photonic filter by machine learning technique," *J. Lightw. Technol.*, vol. 38, no. 19, pp. 5302–5310, 2020.

[23] J. Li, L. Xuan, X. Zhang, T. Feng, and L. Xi, "Analysis of the stability and optimizing operation of the single-side-band modulator based on re-circulating frequency shifter used for the T-bit/s optical communication transmission," *Opt. Exp.*, vol. 18, no. 17, pp. 17597–17609, 2010.

[24] H. Ou, H. Fu, D. Chen, and S. He, "A tunable and reconfigurable microwave photonic filter based on a raman fiber laser," *Opt. Commun.*, vol. 278, no. 1, pp. 48–51, 2007.

[25] J. Mora, A. Ortigosa-Blanch, D. Pastor, and J. Capmany, "Tunable microwave photonic filter free from baseband and carrier suppression effect not requiring single sideband modulation using a mach-zenhder configuration," *Opt. Exp.*, vol. 14, no. 17, pp. 7960–7965, 2006.

[26] J. Yao and Z. Jiao, "Passband-switchable and frequency-tunable dual-passband microwave photonic filter," *J. Lightw. Technol.*, vol. 38, no. 19, pp. 5333–5338, 2020.

[27] T. X. Huang, X. Yi, and R. A. Minasian, "Single passband microwave photonic filter using continuous-time impulse response," *Opt. Exp.*, vol. 19, no. 7, pp. 6231–6242, 2011.